DIABATIC FORCING OF THE TROPICAL ATMOSPHERE IN A GENERAL CIRCULATION MODEL

David Gregory
Meteorological Office,
Bracknell, United Kingdom

1. Introduction

In the UK Meteorological office an 11-layer general circulation model has been used in climate research for several years. Recently a modified convection scheme has been tested which incorporates an improved representation of evaporation within convective downdraughts. During July of an annual cycle integration with the new scheme (experiment EVKS) an anomalous circulation develops over the west Pacific. The feature is quasi-stationary lasting for 60 days and is associated with enhanced convective rainfall. Cyclonic flow exists at 850 mb with the reverse flow at 200 mb. The control experiment (CW4A) with the standard convection scheme does not exhibit this feature. Both experiments are analysed to obtain details concerning the circulation and the mechanism by which it is formed. Results indicate the importance of representing correctly the interaction of convection and transient (planetary) waves in the tropics if general circulation models are to capture the climatology of the atmosphere.

2. The Model

Basic details of the 11-layer model are given by Slingo and Pearson (1985) and detailed documentation is provided in Slingo (1985). Only a brief summary is provided here. A horizontal 2.5 x 3.75 degree latitude-longitude grid is used with sigma co-ordinates in the vertical. Primitive equations are employed with centred space differencing and a leap frog time integration scheme.

Boundary layer processes are represented by a diffusive scheme, calculations being carried out in terms of conserved variables (liquid water temperature and total water content) (Smith (1985)). Diffusion coefficients are stability-dependent. Cloud liquid water/ice content is represented explicitly in the model and is obtained (together with amounts of high, medium and low layer cloud) from a statistical cloud model based upon the work of Sommeria and Deardorff (1977). A parameterization based on that of Sundqvist (1978) is used to calculate the large-scale rainfall rate. Smith (1985) describes the scheme in detail.

An interactive radiation scheme is employed, radiative fluxes being calculated from the temperature and moisture profiles together with cloud amounts (Slingo and Wilderspin (1985)). Convection is represented by a penetrative scheme which is described in the following section. Mean orography is used together with a representation of orographic gravity-wave drag (Slingo and Pearson (1987)). Land surface processes are represented by an interactive scheme (Carson (1982a)), surface temperature, soil moisture content and snow depth being allowed to vary.

3. The convection scheme

A penetrative convection scheme is used in the model and is fully documented in Slingo (1985). Here only a brief description is provided, concentrating upon points relevant to the experiments described in this paper.

The scheme is based upon parcel theory, modified by en/detrainment. The parcel represents an ensemble of buoyant plumes, each of differing characteristics. Parcel values of temperature, mixing ratio and mass flux are thus averages over the ensemble.

For a column of atmosphere, working from the surface upwards, each layer of the model is tested until one is found in which air with a slight excess buoyancy (0.2K) is still buoyant at the next layer after ascent, taking entrainment of environmental air into consideration. If the buoyancy exceeds a lower limit (0.2K) the convective process is initiated. The initial mass flux (M_I) of the parcel is proportional to the excess buoyancy,

$$M_I = 3.33 \times 10^{-7}(2\Delta t)(\theta^P_{v_{k-1}} - \theta^e_{v_{k-1}} - 0.2)/\Delta\sigma_{k-1/2} \qquad (1)$$

where θ^P_v is the virtual potential temperature (K) of the parcel

θ^e_v is the virtual potential temperature (K) of the environment

Δt is the timestep of the model

and $\Delta\sigma_{k-1/2} = \sigma_k - \sigma_{k-1}$ (k decreasing with height).

M_I is not allowed to exceed the thickness of the shallowest model layer (layer 11, the bottom layer). Also if M_I does not exceed $3.33 \times 10^{-7}(2\Delta t)$ convection is not initiated.

Ascent continues upward, the parcel entraining environmental air at level σ at the rate of $4.5\sigma\Delta\sigma$. Mixing detrainment occurs at a third of this rate. Detrainment at zero buoyancy (forced detrainment) relative to cloud environment occurs only when necessary to maintain minimum excess buoyancy (0.2K). However this process allows buoyancy to increase indefinitely and so is limited by two constraints which terminate the convective process. Firstly a parcel cannot ascend higher than an undilute parcel from the starting level. Secondly if after detrainment the mass flux is less than the minimum initial value defined above, the parcel is assumed to be destroyed by entrainment. In the event of the termination of convection the parcel detrains at neutral buoyancy in layer k and at parcel values in layer k-1.

The plume interacts with its environment through en/detrainment of air and environmental subsidence which compensates the parcel's upward mass flux. Detrainment of cloud liquid water and the evaporation of falling precipitation also effect the environment.

In the experiments reported in this paper, two different versions of the convection scheme are used which treat these processes differently.

(a) Standard scheme: precipitation forms when cloud depth exceeds a critical value (4.0 km over land, 1.5 km over sea (or if the parcel temperature falls below 263K)) and the cloud condensate (X^P) exceeds a critical value (Xmin = 1g/Kg). If these criteria are not met, then the condensate is retained within the parcel allowing the possibility of detrainment and evaporation within cloud environment. If the criteria are met the precipitation rate is given by

$$P_k = (X^P_{k-1} - Xmin)M_{k-1}(10^2 p_*/g) \qquad (1)$$

where p_* is the surface pressure in mb. Xmin of the condensate is retained in the parcel and transported upward.

Precipitation is only allowed to evaporate below cloud base (if the air is not saturated) the amount reaching layer k from layer k-1 being given by,

$$J_k = J_{k-1} \exp[-10\Delta t p_* \Delta\sigma_k [q_s(T^e_k) - q^e_k]/J_b g] \qquad (2)$$

where J_b is the total precipitation falling from cloud base and q_s is the saturation mixing ratio.

(b) Modified convection scheme: precipitation forms when cloud condensate exceeds a critical value (1g/kg over sea, 2g/kg over land). An amount Xmin (1g/kg) is retained by the parcel, the precipitation rate being given by eqn (1). If cloud top is in layer 8 ($\simeq$ 730 mb) or above then evaporation occurs in all layers through which it falls, modelling the evaporation which occurs in deep convective downdraughts. When cloud top is below this evaporation is only

allowed below cloud base. The evaporation scheme is a development of one proposed by Rowntree (personal communication (1986)) based upon the work of Kessler (1969) with some suggestions of Lin et al (1983) being incorporated. Different formulae are used for ice and liquid water. The precipitation rate at the bottom of a layer (S_B, R_B) of thickness $\Delta\sigma$, temperature T and of mixing ratio q is given by,

$$\text{ICE} : S_B = \left[S_T^{0.2647} - 5.949\times10^{5}\, A_S(T)(q_S(T)-q)\Delta\sigma\,(p_*/g)\right]^{3.7779}$$

$$\text{WATER} : R_B = \left[R_T^{0.22195} - 2.504\times10^{5}\, A_R(T)(q_S(T)-q)\Delta\sigma\,(p_*/g)\right]^{4.50552}$$

(with p_* in mb). $A_S(T)$ and $A_R(T)$ are quadratics in temperature which arise because of the variation of the diffusivity of water with respect to temperature especially below 0°C.

4. Comparison of the model with climatology

Before the impact of changes in the specification of diabatic heating is considered, the climatology of the standard model described in section 2 is discussed. The simulation (hereafter referred to as CW4A) is an annual cycle integration and the month of July is chosen for comparison (the integration having started at the beginning of September of the previous year). The initial conditions were taken from a previous integration of the model. For the purposes of comparison the observed climatology is taken to be the mean July for 1983 to 1986 from the Meteorological Office operational archive.

Fig. 1 shows a sigma-latitude cross section of the zonal mean wind (u) for the model and "climatological" July. The mid-latitude jet streams in the upper troposphere are located reasonably well by the model (around 200 mb) although central magnitudes are over-estimated in both hemispheres. Upper level easterlies over the tropics extend too far down towards the surface (the 5 ms^{-1} contour to 500 mb compared to 400 mb in the

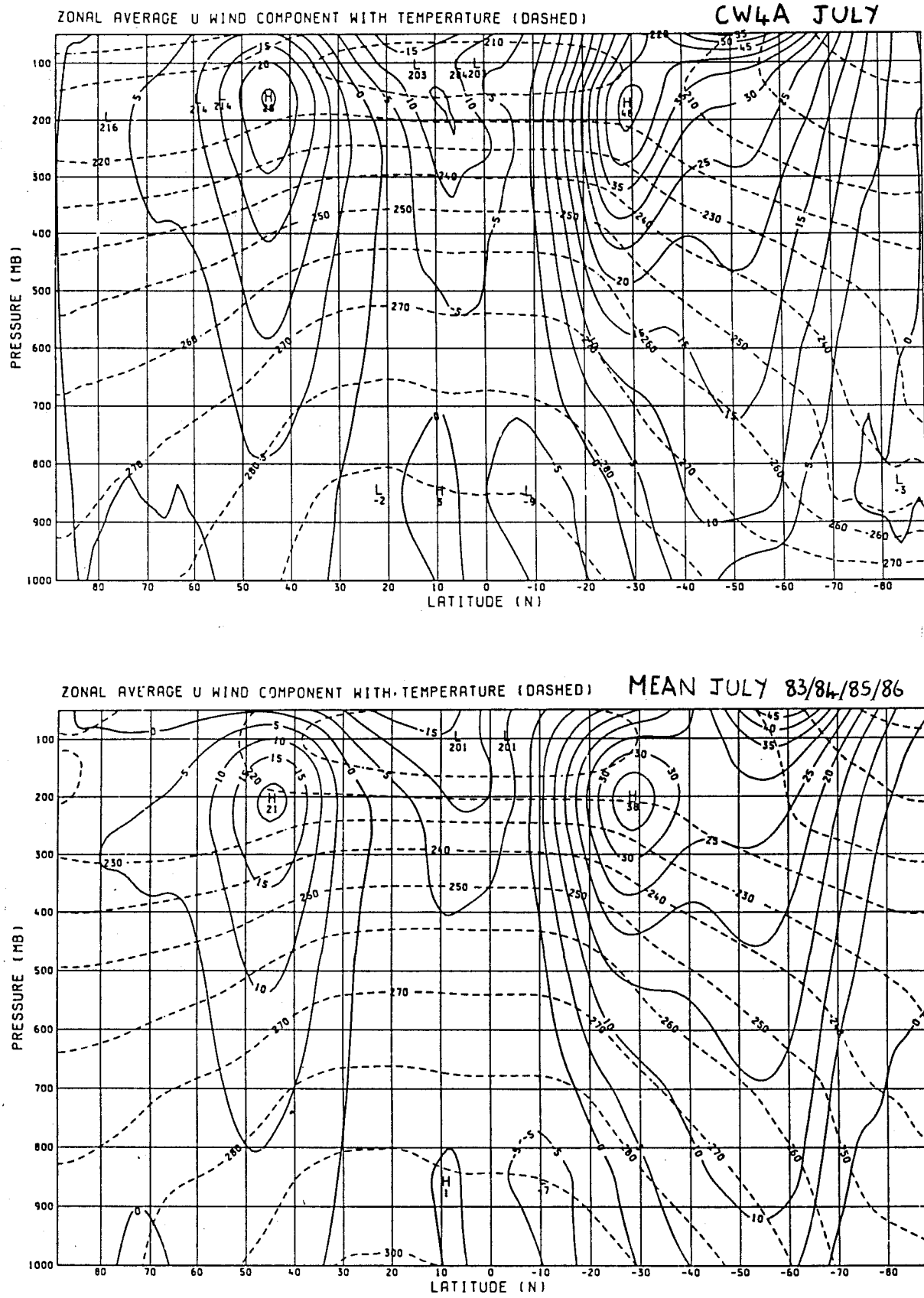

Fig. 1. Height-latitude cross-sections of zonal mean zonal wind (full line) and temperature (dotted line) for CW4A (July) and observed July climatology.

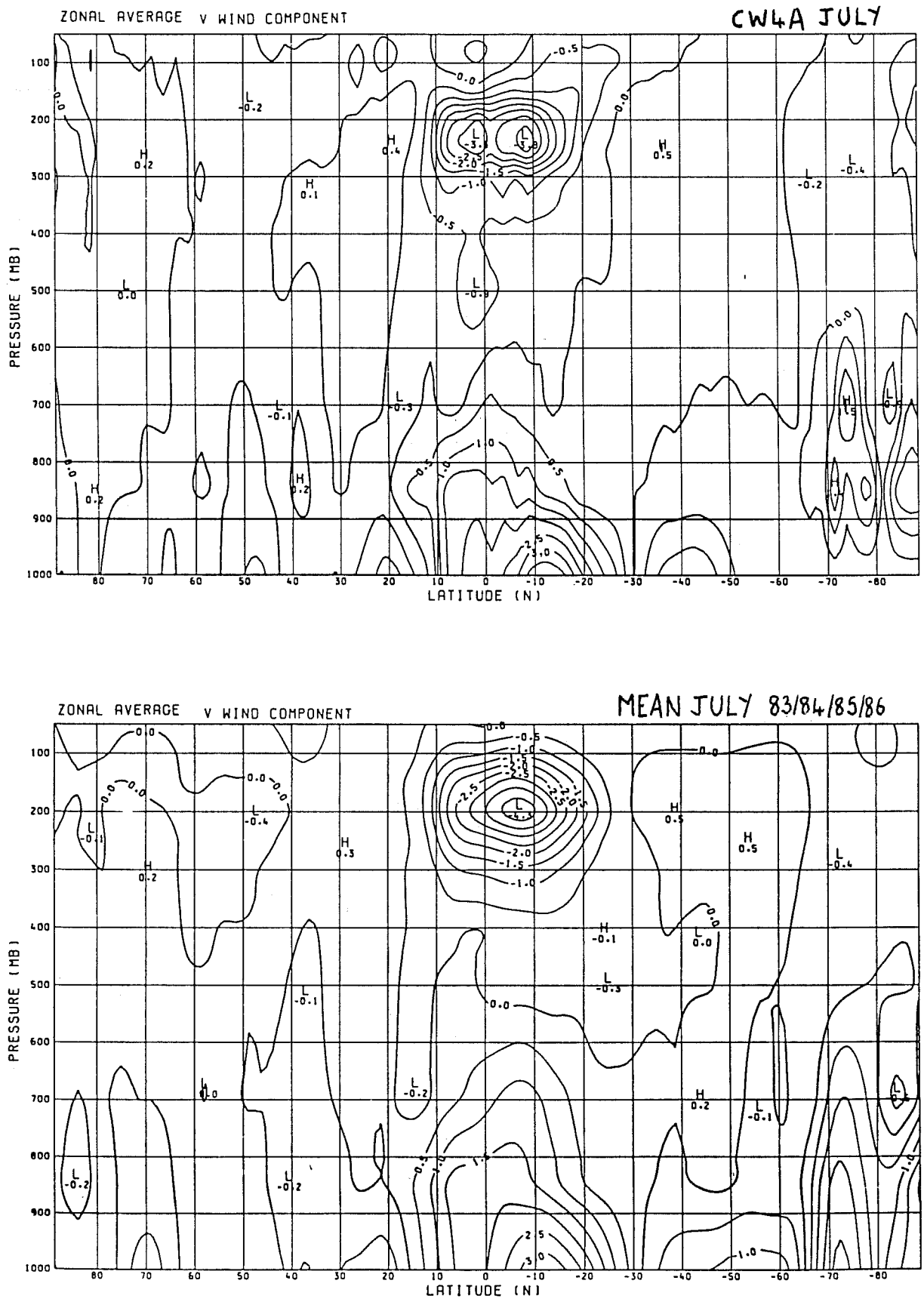

Fig. 2. Height-latitude cross-sections of zonal mean meridional wind for CW4A (July) and observed July climatology.

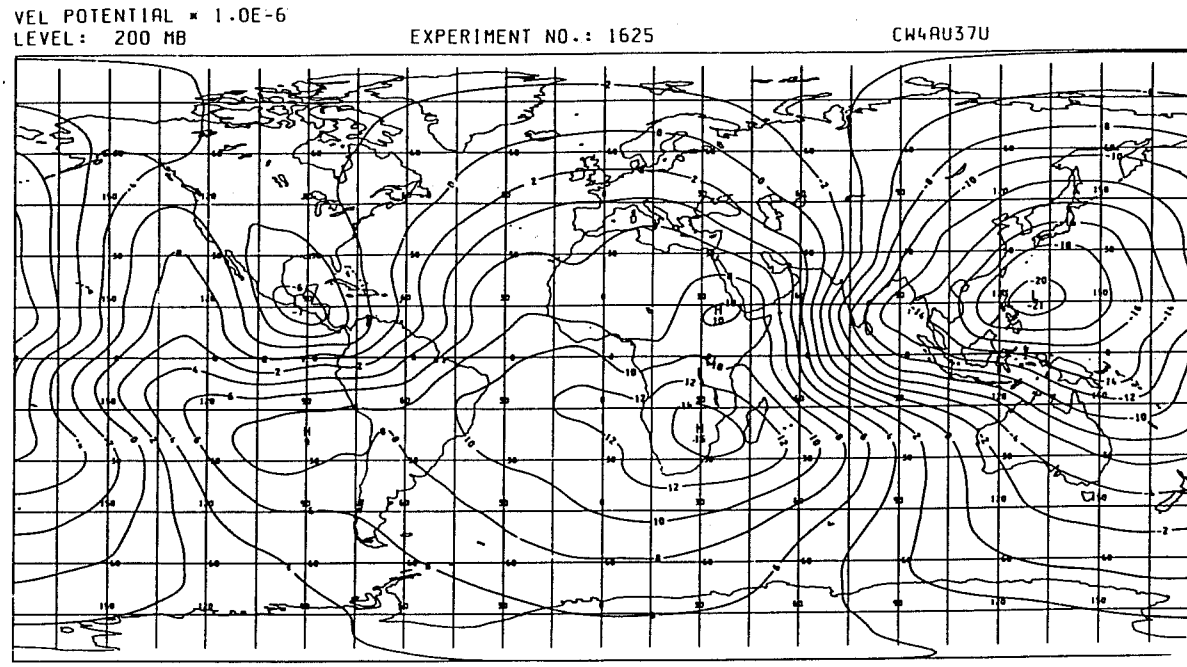

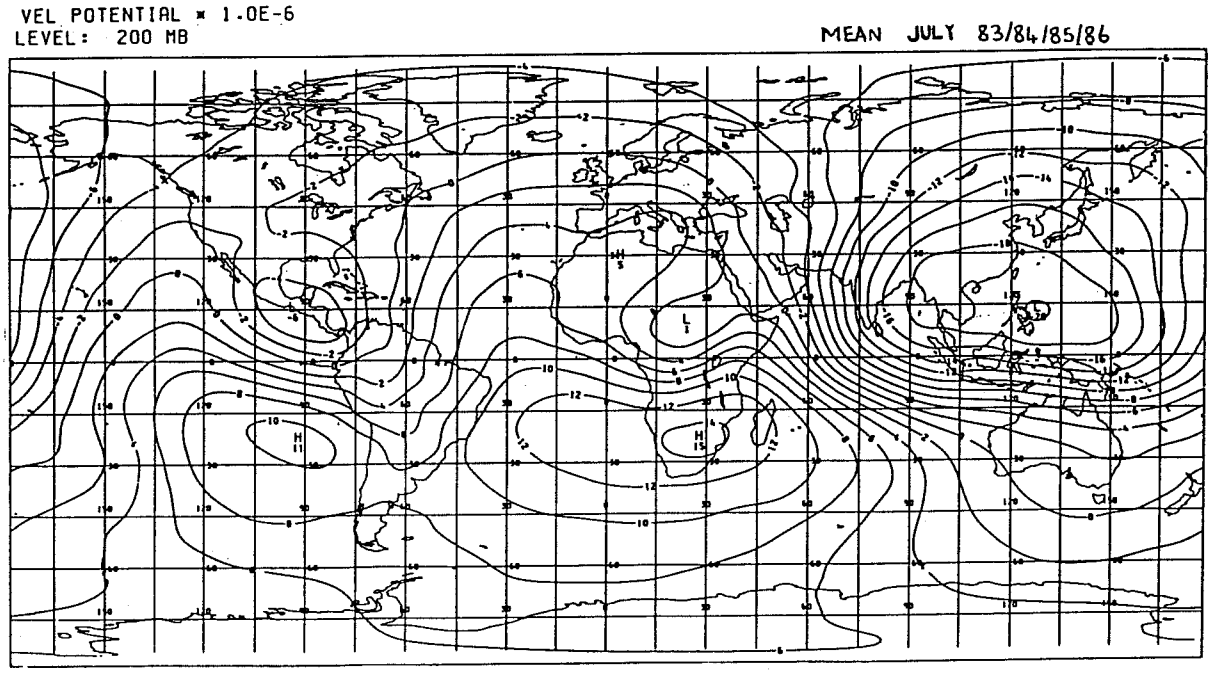

Fig. 3. Velocity potential for CW4A (July) and observed July climatology at 200 mb.

observations). Surface easterlies also appear too intense by 2 ms^{-1}. The zonally averaged temperature field is also included in fig. 1. The decrease of temperature with height appears reasonable in the tropics but too great over the poles, enhancing the north-south temperature gradient and resulting in tropospheric winds being too large in mid-latitudes . Fig. 2 shows zonally averaged meridional velocity (v). The Hadley circulation is clearly seen, being most evident in the winter hemisphere. A minimum in the meridional velocity is seen just south of the equator in the return flow in the upper troposphere associated with too extensive a Pacific dry zone which extends into the Indian Ocean (fig. 5). The inflow circulation is reasonably represented although the stagnation level of the circulation is 100 mb lower than observed.

The Hadley circulation is driven by diabatic heating in the tropics (mainly convection). However zonal means do not give the full picture as much zonal asymmetry exists. Fig. 3 compares the velocity potential at 200 mb (χ_{200}) for the model and climatology. The main areas of ascent (positive $\nabla^2\chi$) (W. Pacific, Central America) are well represented together with areas of descending motion (the sub-tropical highs). The central magnitude of the pattern is realistic although some difference in the geographical distribution is seen. Over the western Pacific the $-18\times10^{-6}s^{-1}$ contour extends further west in the observations although some of this can be accounted for by the geographical variation of the centre of the pattern from year to year (the central magnitude showing only a 10% variation). Greater troughing is observed over South America in the observations which appears to be reflected in the precipitation field over this region (fig. 5). In the summer the model produces much less precipitation than climatology suggests. However despite these differences the Walker and Hadley circulations are clearly seen.

The 850 mb wind field (fig. 4) clearly shows the features expected for this time of year. The Monsoon jet is well located although too little troughing occurs over the Bay of Bengal. Its maximum magnitude is too low and the jet extends too far east over the west Pacific. Easterlies over the equatorial Atlantic and Pacific are too strong. Comparison of the model precipitation field (fig. 5) to the climatology due to Jaeger (1976)

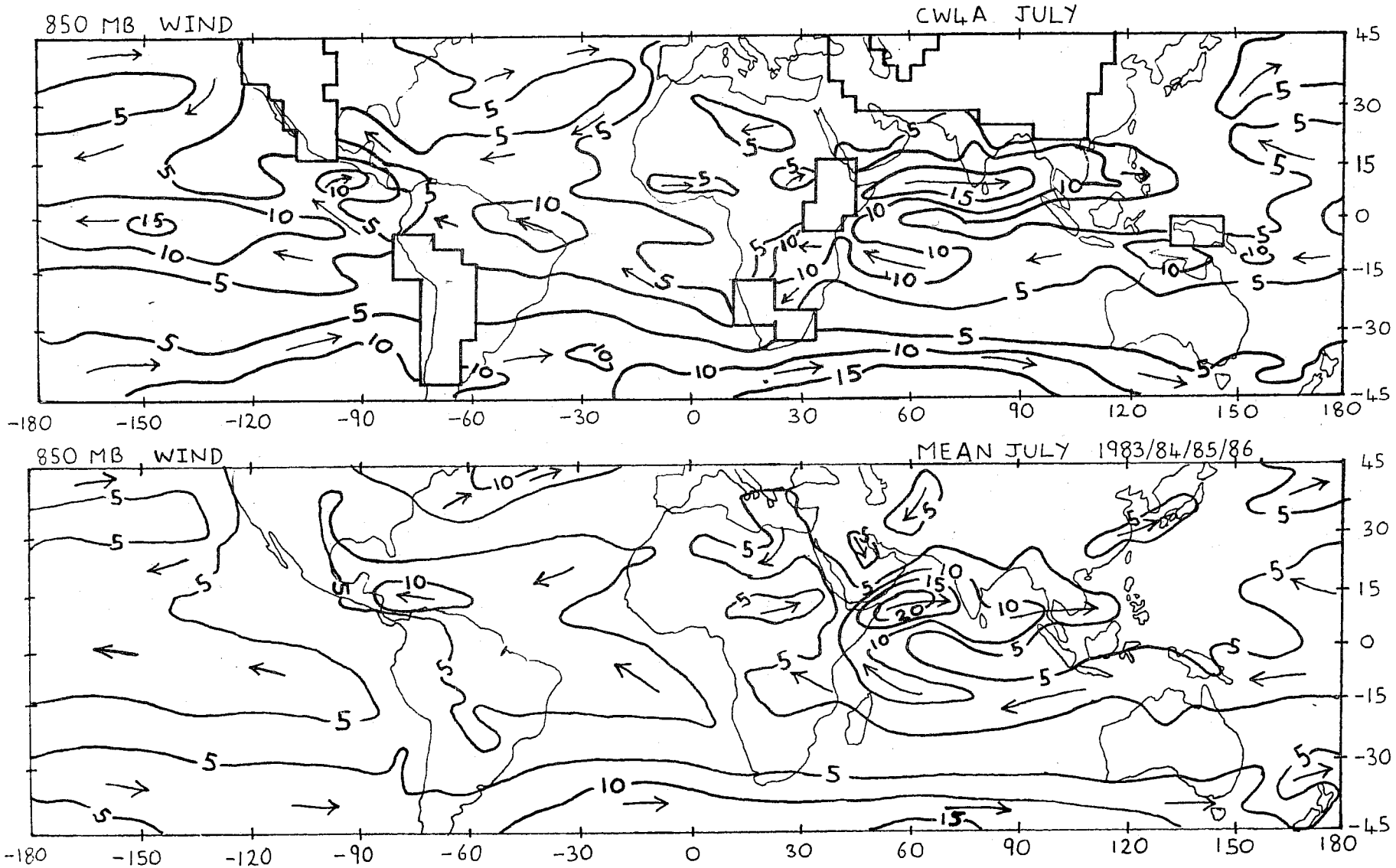

Fig. 4. $\underline{V}$ at 850 mb for CW4A (July) and observed July climatology.

TOTAL RAINFALL.
CONTOUR INTERVAL 0.1. 1.0. 2.0. 5.0. 10.0. 20.0. AND
EVERY 20MM ABOVE. SHADED ABOVE 5.0MM/DAY
LEVEL: SURFACE

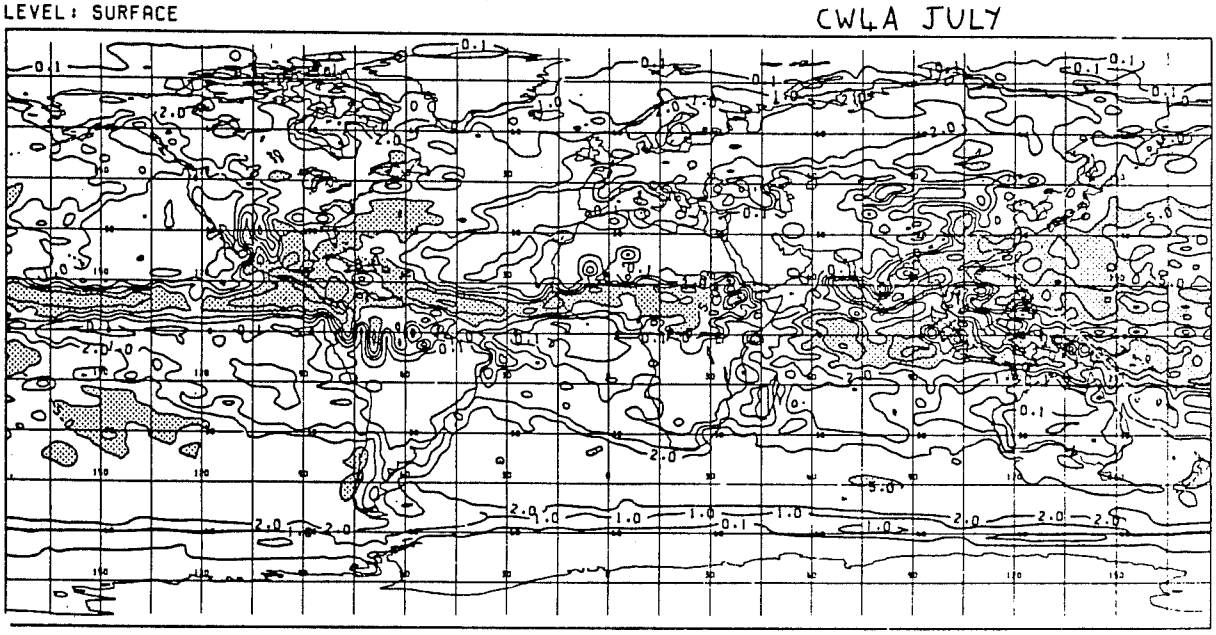

CLIMATOLOGICAL MEAN RAINFALL. JAEGER(1976)
CONTOUR INTERVAL 0.1. 1.0. 2.0. 5.0. 10.0. 20.0. AND
EVERY 20MM ABOVE. SHADED ABOVE 5.0MM/DAY
LEVEL: SURFACE

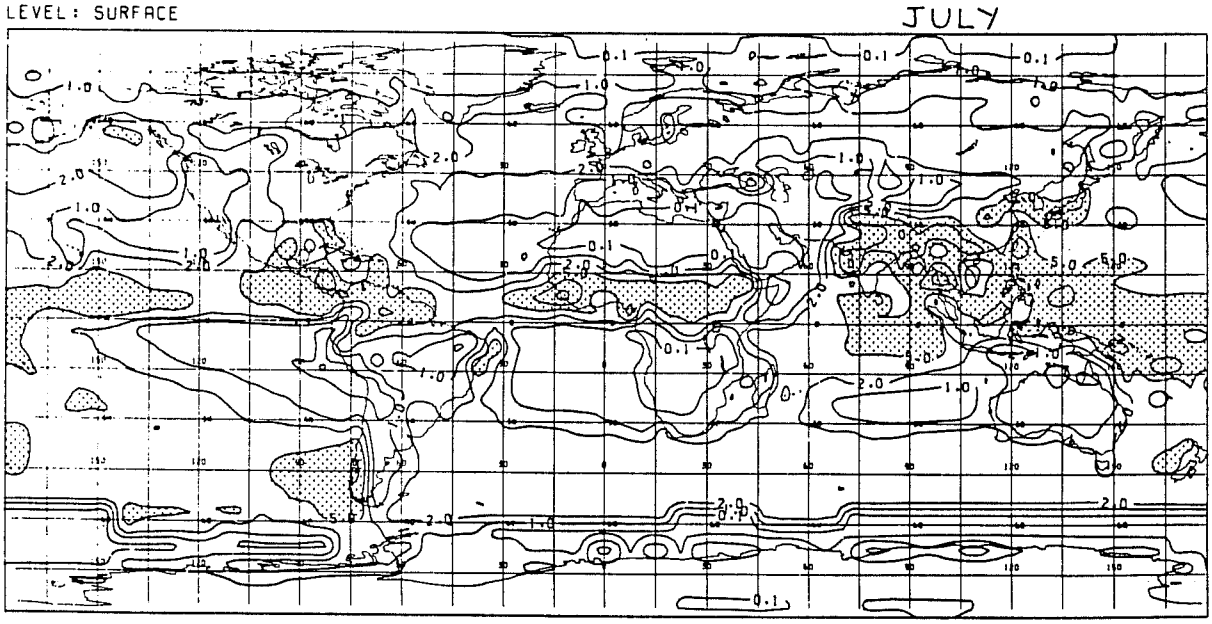

Fig. 5. Surface precipitation for CW4A (July) and observed July climatology (Jaeger).

is reasonable over much of the globe. However peak magnitudes are in disagreement the model producing too much rain over oceans and not enough over land. South America is too dry (as commented above) as is India. The east Pacific equatorial dry zone also extends too far west into the western Pacific and Indian Ocean. This may be linked to errors in the sea surface temperature in this region.

Although the control simulation does have certain deficiencies as discussed, overall it provides a reasonable simulation of the tropical circulation and so proves useful for a study of the impact of the parameterization of diabatic heating.

5. Impact of modified convection scheme

Experiment EVKS was run through an annual cycle parallel to CW4A (starting from the same initial data) to study the impact of the modified convection scheme. The main impact is found in the tropics. Convective and high cloud cover were increased, global cloud cover increasing by 2% to 55%, with albedo increasing by 1%. Over the tropical oceans the lowest model layer is warmer and drier due to a reduction in the evaporation of precipitation, while the atmosphere above this is wetter (0.5g/kg globally in the tropics) due to increased evaporation of convective precipitation. Over the west Pacific and Indian Oceans 850 mb temperatures are 1 to 2K cooler.

An interesting anomalous circulation develops over the west Pacific during July of EVKS. The 850 mb Monsoon jet (fig. 6) extends from South East Asia over the Philippines and out into the central north Pacific Ocean, differences in wind speed being up to 19 ms^{-1}. To the north of the westerly jet weaker easterlies are seen. At 200 mb a reverse anticyclonic flow develops. Differences over the remainder of the tropics are small. At 200 mb lower values of velocity potential are seen over the Western Atlantic (fig. 7) with higher values over Central America implying an enhanced Walker Circulation (increased subsidence over the Sahara and Southern Indian Ocean are also implied). Rainfall over the western Pacific

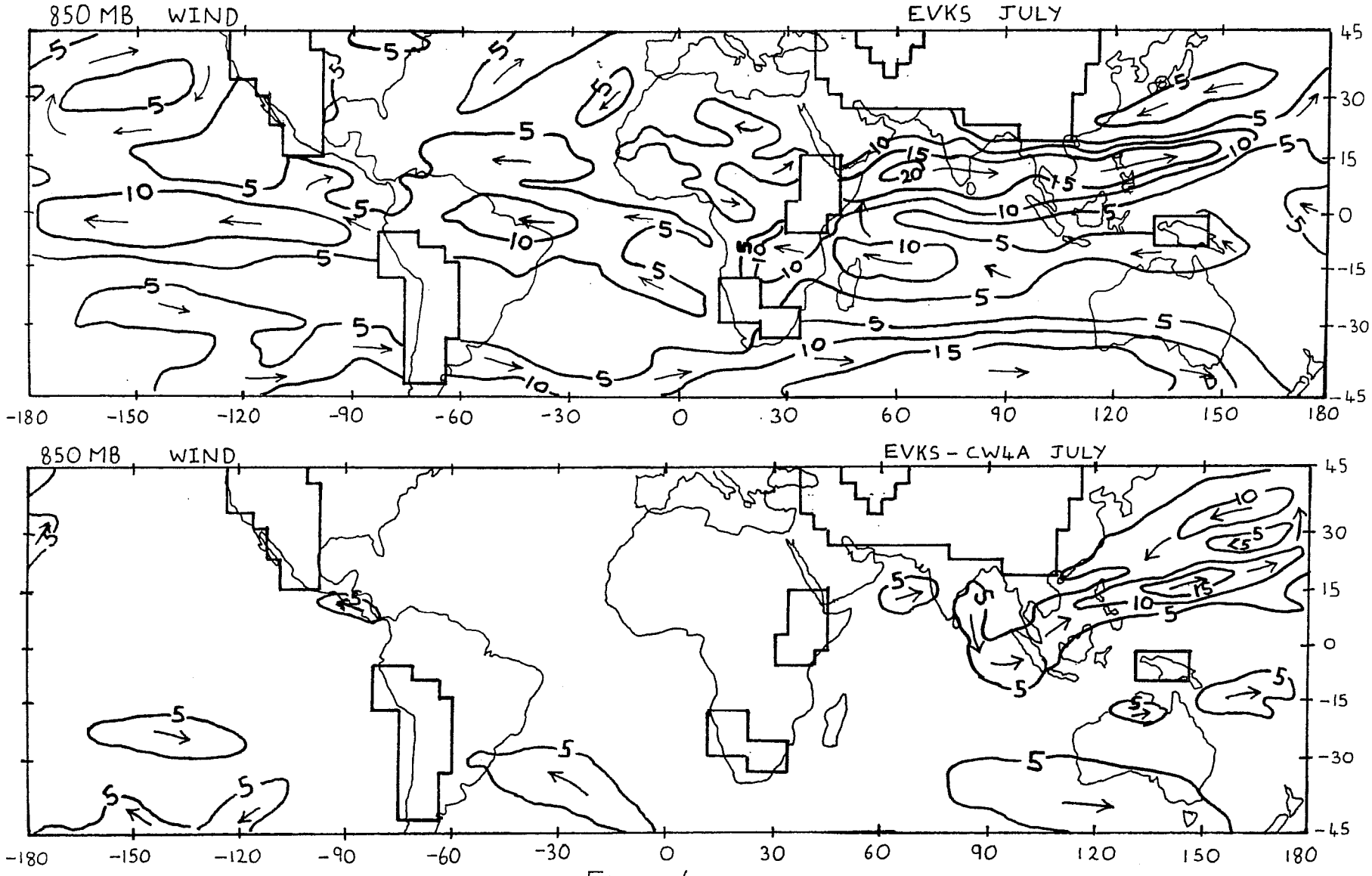

Fig. 6. $\underline{V}$ at 850 mb for EVKS and EVKS-CW4A for July of an annual cycle integration.

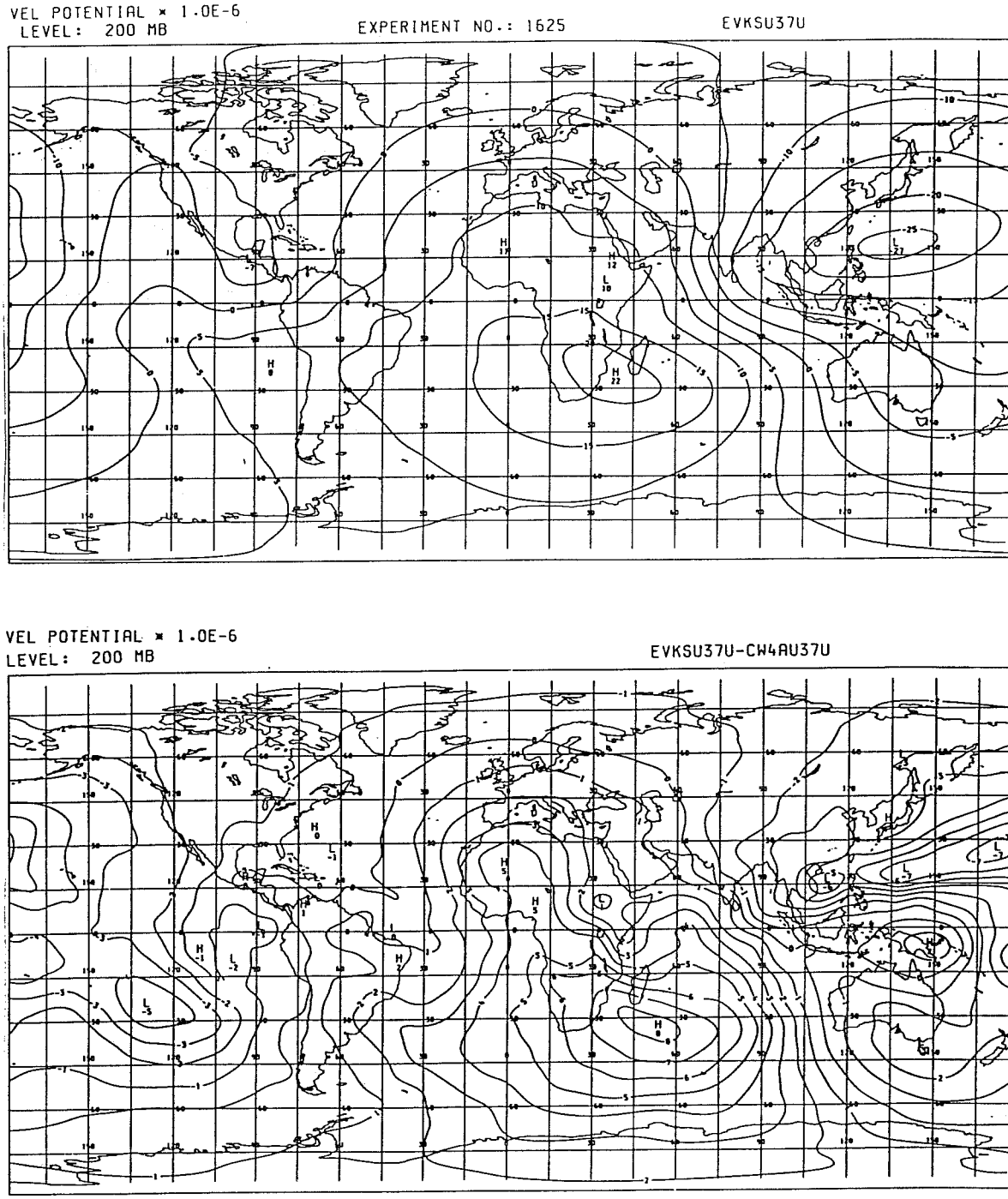

Fig. 7. Velocity potential at 200 mb for EVKS and EVKS-CW4A for July of an annual cycle integration.

(fig. 8) increases to over 40 mm/day, an increase of 30 mm over CW4A. Smaller increases are seen in the ITCZ over oceans while decreases of up to 10 mm/day occur over Africa.

The relationship between wind, pressure and precipitation can be seen more clearly in fig. 9 which shows these fields over a limited area of the Indian Ocean and West Pacific. The westerly jet lies to the south of a trough extending out of South East Asia. The band of rain is clearly associated with the jet (rain greater than 5 mm/day is shaded).

The anomalous circulation is very similar to that studied by Phlips and Gill (1985) using a simple linear model of the atmosphere. Fig. 9c (fig. 11b of their paper) shows the circulation induced by an elongated heat source placed north of the equator in the presence of a mean westerly wind. The similarity to the feature found in the GCM experiment is obvious. Hence the anomalous flow over the west Pacific is clearly identified as being caused by enhanced latent heat release over the region.

Similar anomalous circulations have been identified in earlier integrations of the 11-layer model. Palmer and Mansfield (1986 II) enhanced sea surface temperatures (SST) in the west Pacific, causing increased convection and forcing a circulation similar to fig. 9c (fig. 16 of their paper). However in these experiments the SST is fixed, the only difference between the integrations being the convection scheme. This suggests that the change is produced internally.

Hartmann et al (1984) investigated the effect of different convective heating profiles upon the Walker circulation using a steady state linear model. Two profiles were used, one representing heating by convective towers peaking in the mid-troposphere, the second a mature cloud cluster with maximum heating in the upper troposphere. They found the Walker circulation was better represented when the mature cloud cluster heating profile was employed. In the GCM a stronger Walker circulation exists suggesting that the two versions of the convection scheme produce differing heating profiles. However this appears not to be the case here. Sensible and latent heat budgets were calculated for the month of July for a small

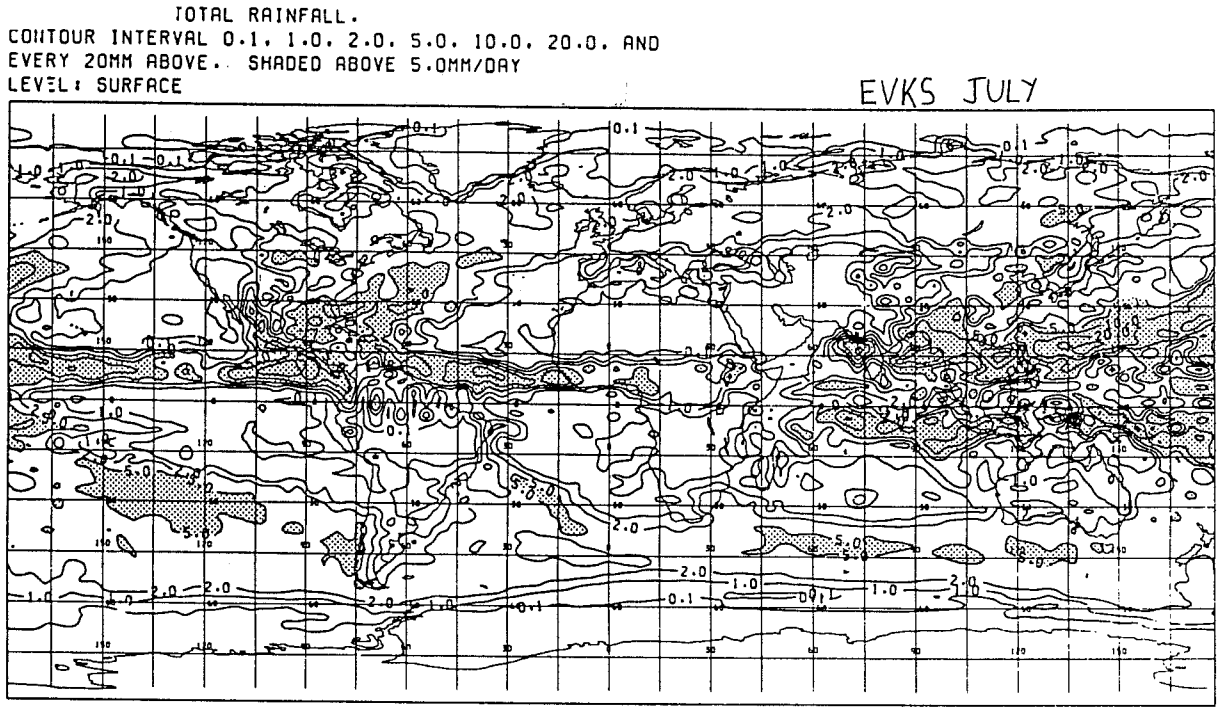

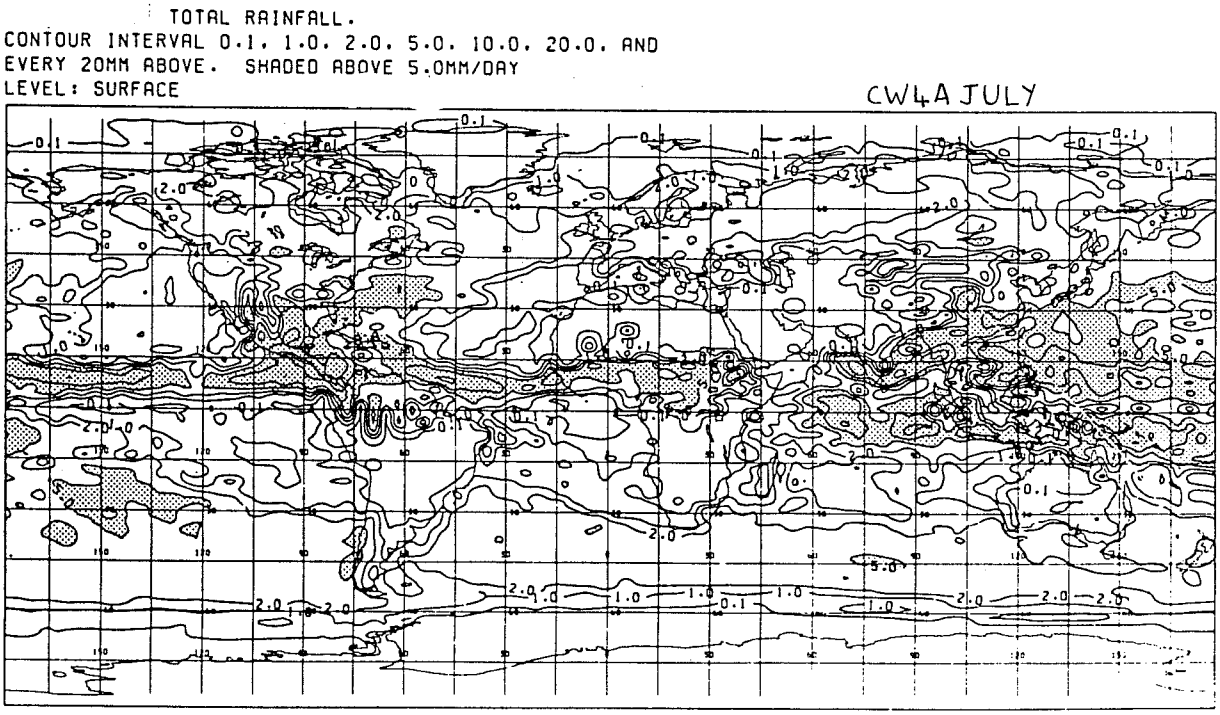

Fig. 8. Surface precipitation for EVKS and CW4A for the month of July.

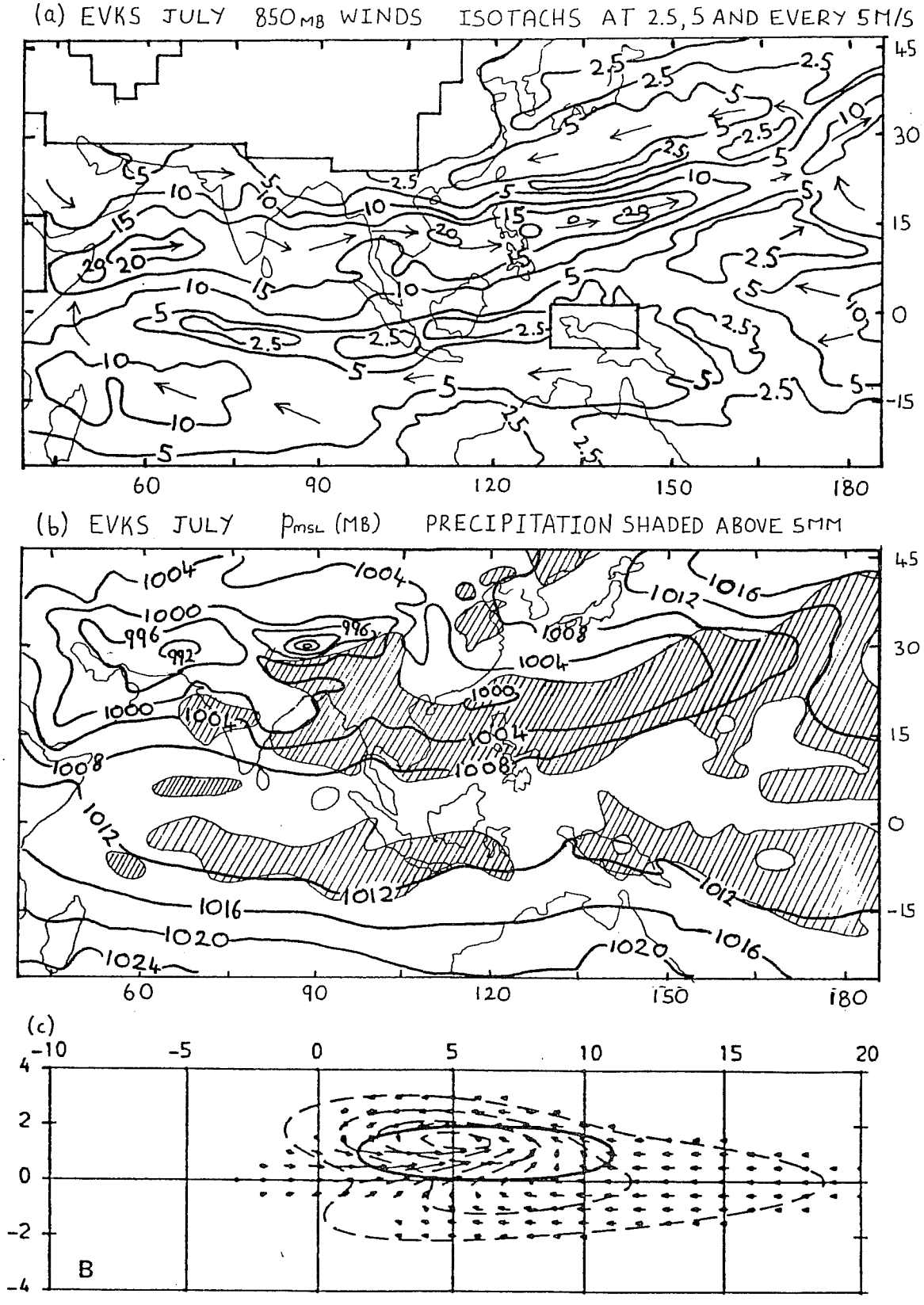

Fig. 9. Flow over the West Pacific and SE Asia for July of EVKS (a) $\underline{V}$ at 850 mb (b) PMSL and surface rainfall greater than 5 mm per day (c) flow produced by an elongated heat source north of the equator in the presence of mean westerly flow (fig. 11b of Phlips and Gill (1985)).

area of the west Pacific between 10 and 20°N and 131.25 and 142.5°W (4 by 3 gridpoints). The core of the jet passed through this region which lies to the east of the Philippines. Profiles of heating due to diabatic and dynamical processes averaged over July are presented in fig. 10. In both CW4A and EVKS convective heating is balanced by dynamical cooling, except in the lowest model layer where warming due to surface fluxes balances cooling due to theevaporation of falling precipitation. Radiation and large-scale rain play only a secondary role.

Both versions of the convection scheme produce heating profiles which peak around 425 mb. This is in reasonable agreement with results of Reed and Recker (1971) obtained over the Marshall Islands (to the east of the present area) (fig. 10c - heating profiles normalised with respect to their peak value). In the lower troposphere the modified convection scheme is in best agreement with the observed profile due to the inclusion of downdraught evaporation. Thus the convection scheme with the "better" heating profile appears to produce a larger systematic error when compared to climatology!

6. Time series over the west Pacific

Time series of several variables averaged over the limited area described in the previous section were created for CW4A and EVKS. Figure 11 shows daily averaged values of zonal velocity at 850 mb for June, July and August for both simulations. A wave with an average period of 18 days is seen in CW4A throughout the three month period, the amplitude of the velocity variation being around 12 ms^{-1}. No similar signal is found in EVKS during June but at the start of July a rapid increase in zonal wind over the west Pacific is seen. This is associated with the onset of the quasi-stationary circulation described previously. During July and August of EVKS a wave feature is seen (with a period of around 18 days) superimposed on a background wind associated with the anomalous circulation. Planetary waves of a similar period have been found to exist

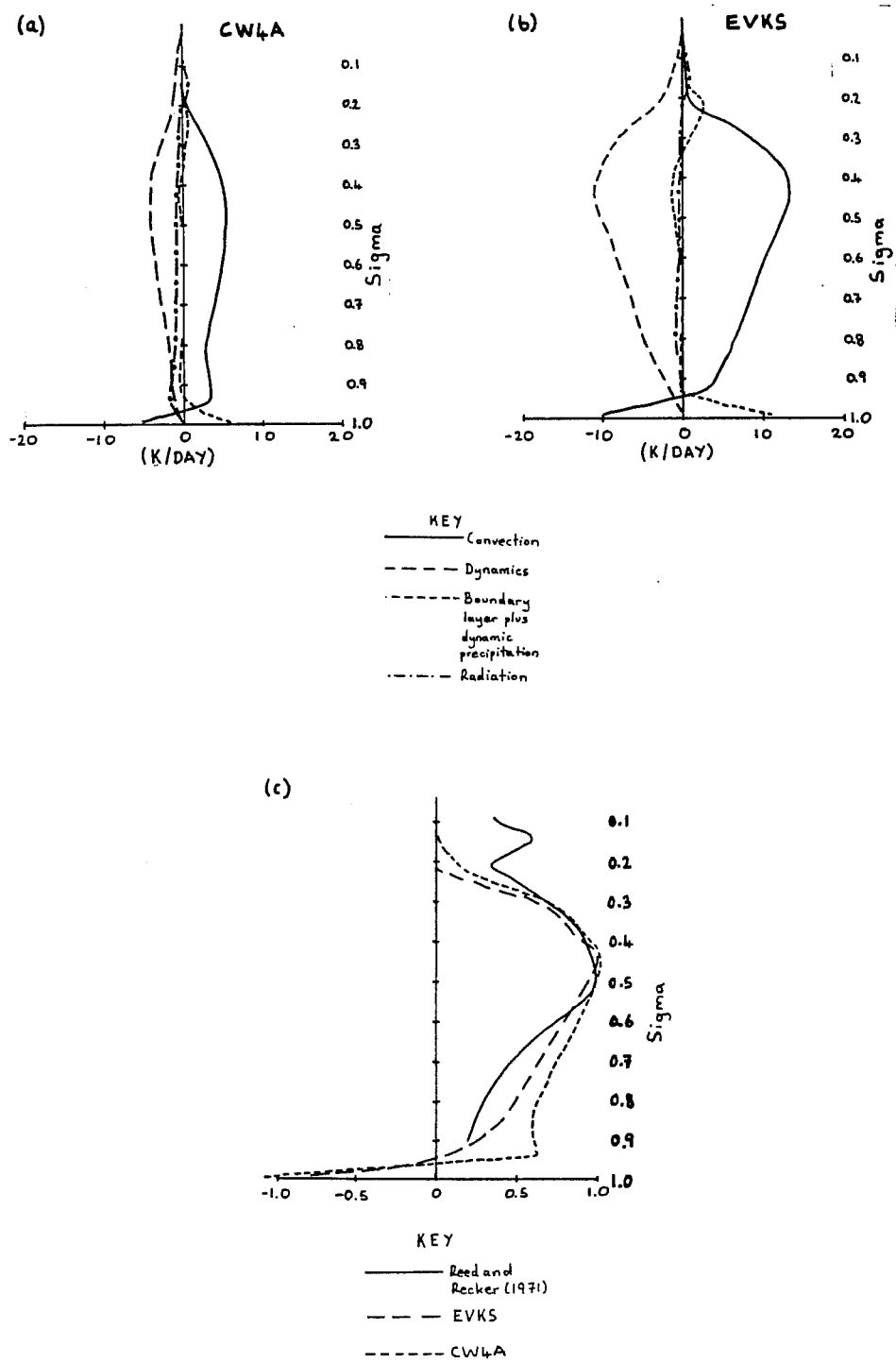

Fig. 10. Profiles of diabatic and dynamical forcing for July averaged over a small area of the West Pacific (defined in text) (a) CW4A, (b) EVKS, (c) Convective heating profiles normalised to maximum heating rates for CW4A and EVKS compared to observed profile.

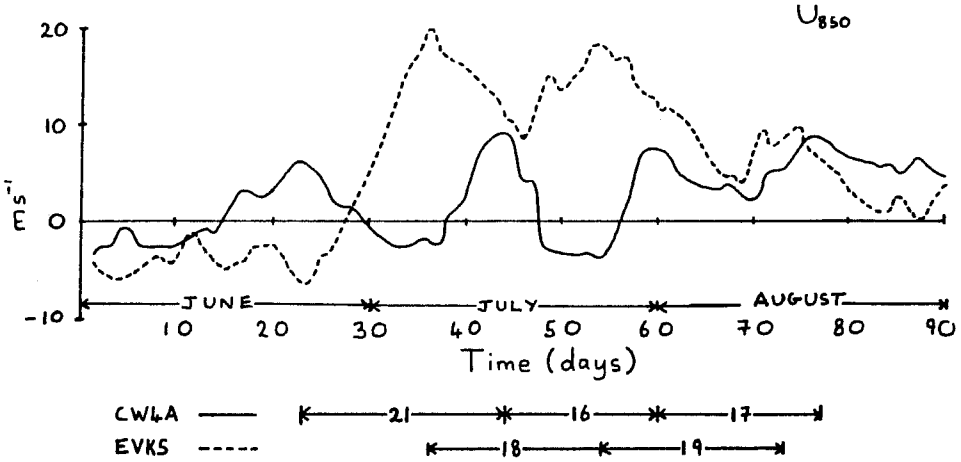

Fig. 11. Time series of U at 850 mb for June, July and August of CW4A (solid line) and EVKS (dashed line) for West Pacific Area.

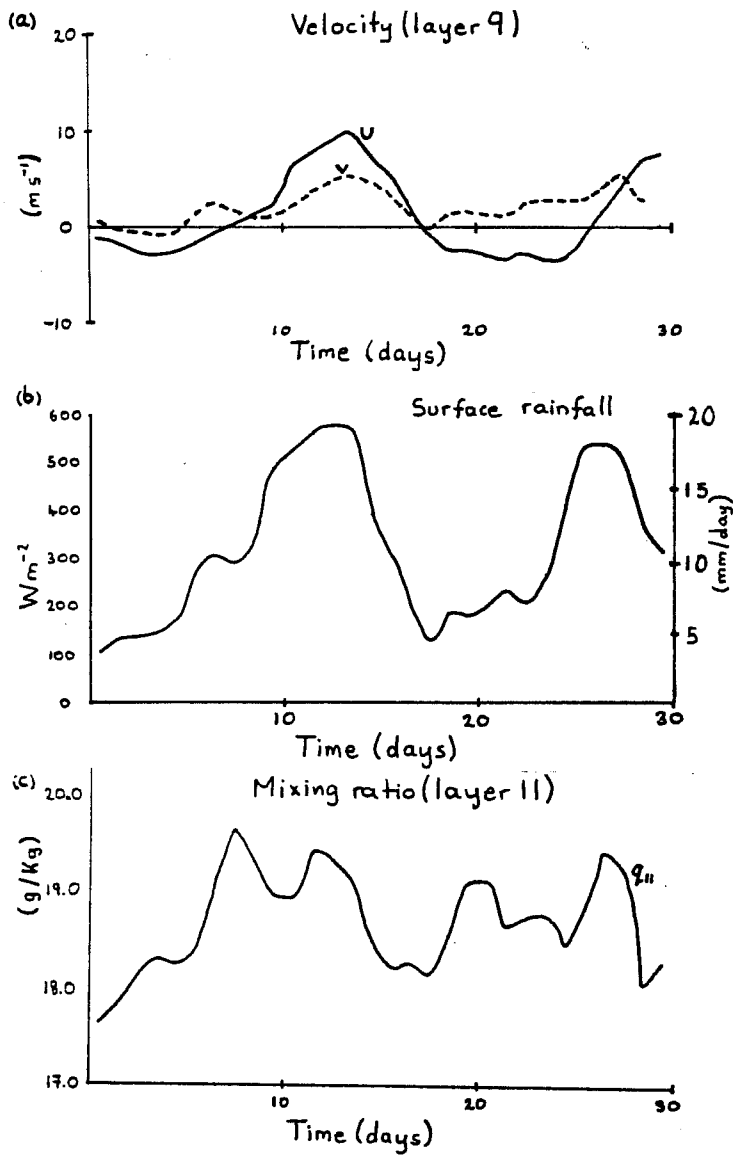

Fig. 12. Time series of (a) U and V at layer 9, (b) convective precipitation and (c) mixing ratio of lowest model layer for CW4A averaged over the West Pacific area for July.

in an aqua-planet version of the 11-layer model by Swinbank et al (1988); the waves propagate in an easterly direction around the globe in the tropics.

Fig. 12 shows daily averaged values of u and v for layer 9 of the model ($\simeq$ 850 mb) together with convective rainfall and mixing ratio for the lowest model layer (layer 11 $\simeq$ 990 mb) for July of CW4A. A wave with a period of around 18 days is found in velocity and rainfall. Mixing ratio peaks around the time of maximum rainfall but the correlation is not exact. The increase in rainfall and velocity is associated with a transient trough which extends out of SE Asia over the Philippines. At its fullest extent the feature resembles the steady state structure seen in July of EVKS (Fig. 9).

The vertical structure of the wave is illustrated in the height-time diagrams for the west Pacific (Fig. 13). (Six hourly averaged values are plotted for the month of July.) The wave is baroclinic in nature with westerlies between σ = .15 and .20 being approximately $^1/_4$ of a wavelength ahead of the low level wind. Convective activity is well correlated to moisture convergence which increases as velocity increases (together with the surface moisture flux). As velocity reduces moisture convergence dries the lower troposphere by up to 3g/kg. Surface moisture flux (not shown) also reduces (from $\simeq$ 6 mm/day at day 15 to $\simeq$ 3.5 mm/day at day 20). Both processes cause convective activity to decrease.

Time series over the west Pacific from EVKS also exhibit a wave with a period of around 18 days (fig. 14). The variation of u through the wave is ~ 10 ms^{-1}, similar to that in CW4A. However a greater background velocity exists (~ 15 ms^{-1}) associated with the quasi-steady state trough over the West Pacific (fig. 9). It is difficult to identify a clear wave in the surface rainfall, several variations on a shorter time scale than 15 days occurring. However the main peaks (~ day 2 and 23) have similar phase to the wind maxima as in CW4A. The mixing ratio of the lowest model layer shows less variation across the wave than in CW4A.

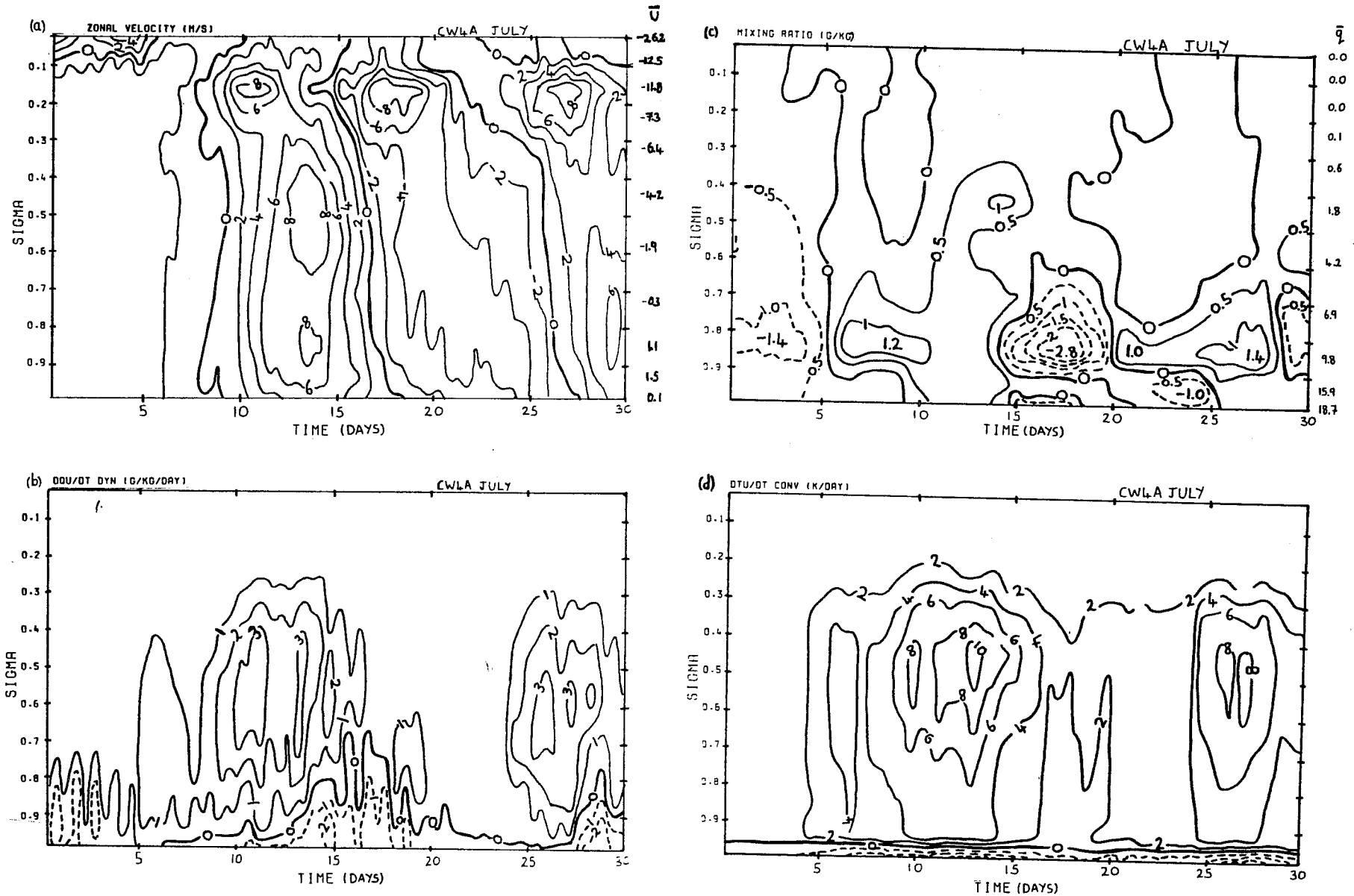

Fig. 13. Time height diagrams of (a) zonal velocity, (b) dynamical moisture forcing, (c) mixing ratio and (d) convective heating for CW4A averaged over the West Pacific area for July.

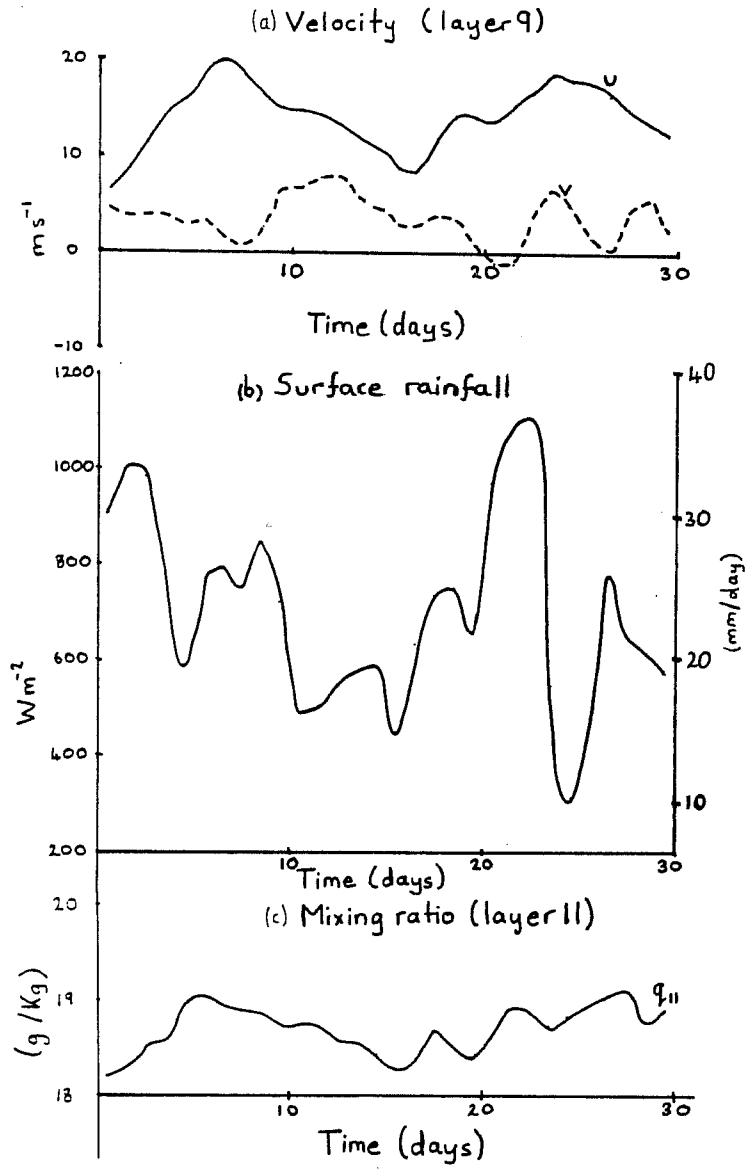

Fig. 14. Time series of (a) U and V at layer 9 (b) convective precipitation and (c) mixing ratio of the lowest model layer for EVKS averaged over the West Pacific area for July.

Fig. 15 shows the evolution of mixing ratio and moisture convergence throughout July of EVKS. Although greater amounts of "noise" are apparent, a similar moistening/drying structure is found associated with the wave (days 8-12 and 20 to 25). As in CW4A, variations in mixing ratio are also similar although not as extreme as in CW4A. As commented above changes in mixing ratio in the lowest 100 mb of the atmosphere are much less than in the same region in CW4A.

The different evolution of the two simulations is due to the modified convection scheme allowing the evaporation of convective precipitation at all levels through which it falls and not just below cloud base (in this instance layer 11) as in the standard scheme. (The change from using a critical depth to a critical water content has little impact upon the simulation.) This produces a wetter atmosphere in EVKS (fig. 16). Below 700 mb EVKS is cooler than CW4A. The greater depth through which the evaporation of convective precipitation occurs also influences the static stability of the two lowest model layers. The difference in potential temperature between layers 10 and 11 is 0.7K in EVKS and 1.3K in CW4A. Thus the atmosphere in EVKS is more unstable with respect to dry ascent. Both CW4A and EVKS have similar mixing ratio in the lowest model layer. Hence buoyancy on lifting a parcel from layer 11 to layer 10 will be greater in EVKS, thus giving a larger initial mass flux and surface precipitation. This greater convective activity supports the steady state feature described over the West Pacific.

The higher static stability of the two lowest model layers in CW4A makes buoyant convection more reliant on a moist lowest layer. Hence convection is modulated by the moisture convergence described previously. In EVKS as the moisture divergence dries the lower troposphere, evaporation of convective precipitation increases and so moderates the changes in the moisture content of the atmosphere. Hence less of a signal is seen in the evolution of mixing ratio. The moister atmosphere plus the low static stability of the lower troposphere allows a greater background precipitation (13 mm/day c.f 2 mm/day in CW4A over the west Pacific) when moisture divergence dries the lower troposphere.

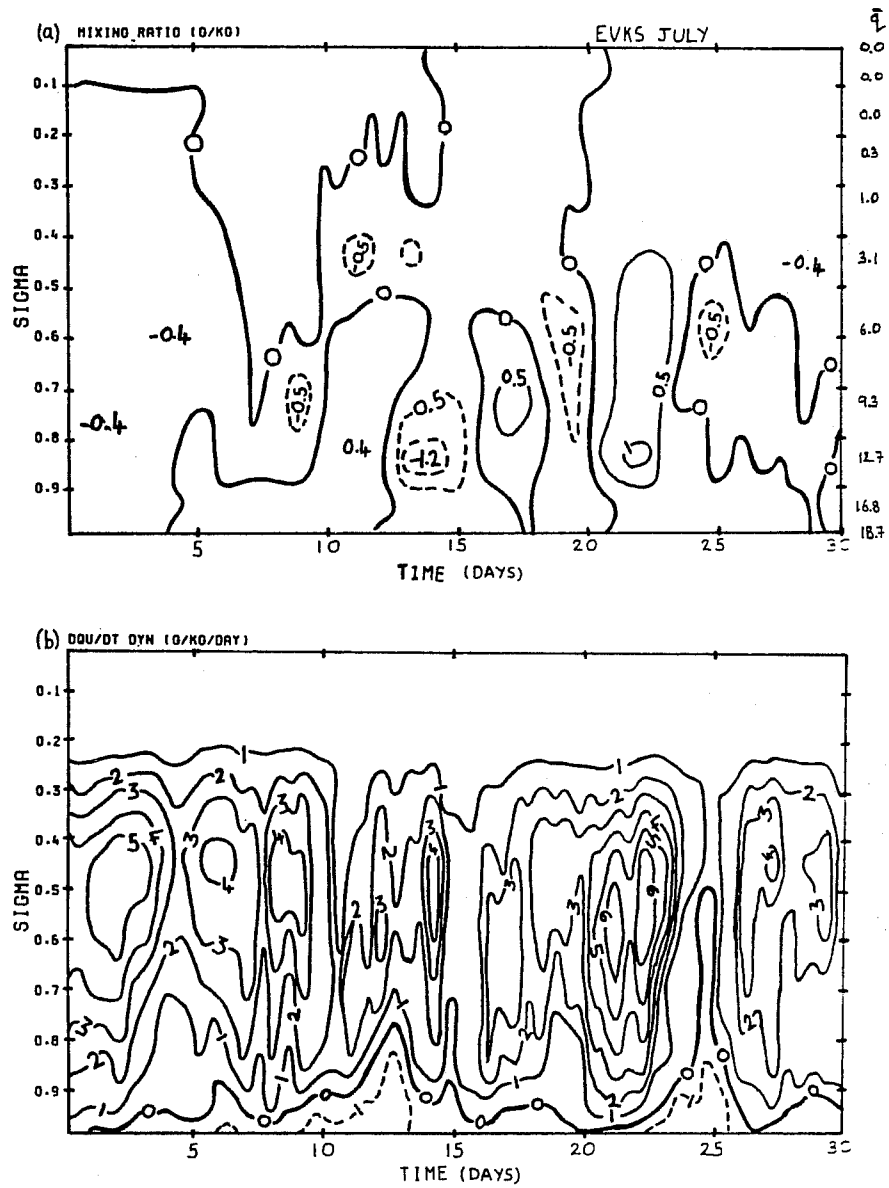

Fig. 15. Time height diagrams of (a) mixing ratio and (b) dynamical moisture forcing for EVKS averaged over the West Pacific Area for July.

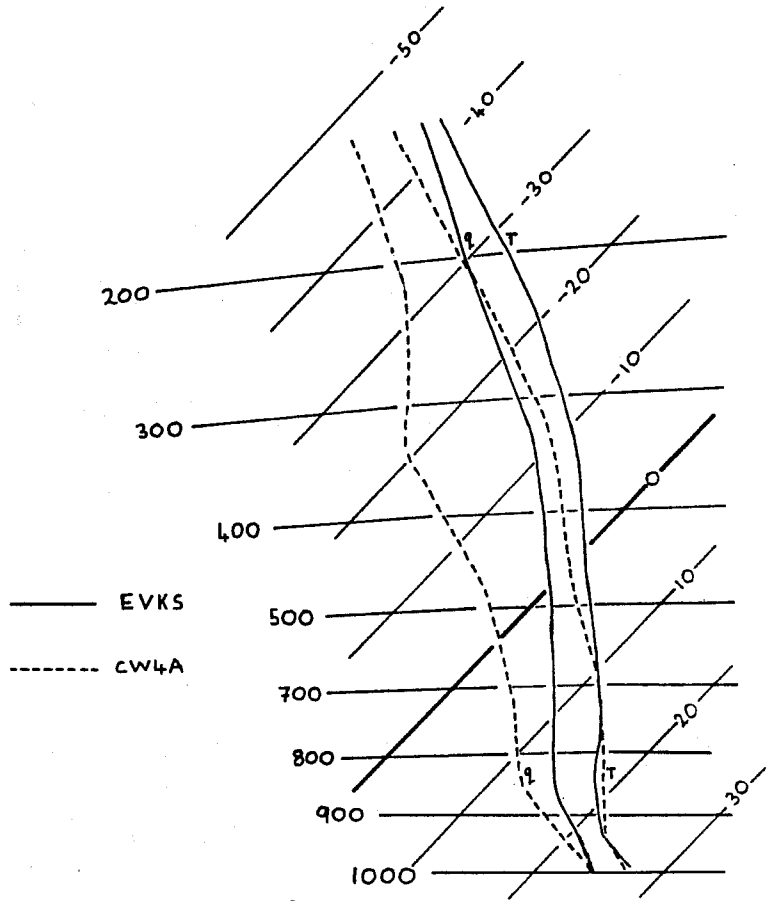

Fig. 16. 30 day mean profiles of temperature and dew point temperature for CW4A (dashed) and EVKS (solid) for July.

7. Hybrid Experiments

Having considered the differences between CW4A and EVKS the question that must still be addressed is what causes the background convection to increase to the point when the quasi-steady state feature can exist over the west Pacific. Two further experiments were carried out, essentially parallel to the July's of CW4A and EVKS but with the convection schemes switched:-

(a) EVT2 : starting from the end of June of EVKS but using the standard convection scheme.

(b) CWT3 : starting from the end of the June of CW4A but using the modified convection scheme.

(a) EVT2

This experiment was integrated forward for 30 days. Over the first 12 days the evolution of velocity in layer 9 (σ = 0.844) is similar to EVKS although surface rainfall is less. After this, decay of the steady state background flow occurs the second wave being only apparent in convective precipitation and not wind speed in layer 9 (fig. 17). This may be caused by the superposition of a decaying background flow and a growing wave. Hence the first half of the integration resembles EVKS the second half, CW4A.

Considering 30 day means over the west Pacific a higher static stability between layer 11 and 10 exists. The difference in potential temperature between the two layers is 1.3K compared to 0.7K in EVKS (see previous section). The lowest model layer is wetter than in EVKS (19.4 g/Kg c.f. 18.7g/Kg) thus compensating for the higher static stability in stability in the calculation of the initial convective mass flux. Hence sufficient latent heating occurs to maintain the steady state circulation over the west Pacific.

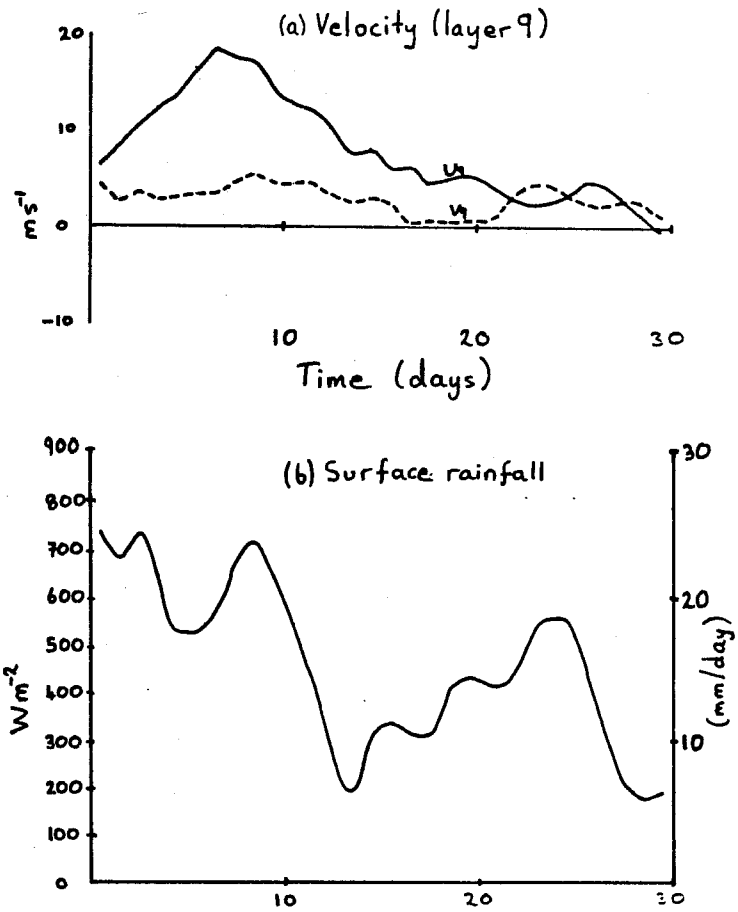

Fig. 17. Time series of (a) U and V at layer 9 and (b) convective precipitation for EVT2 averaged over the West Pacific area for July.

However, as in CW4A, a high static stability causes the convection scheme to be more sensitive to changes in the moisture content of the atmosphere. Hence when moisture divergence dries the atmosphere around day 12 (as in EVKS) convection decays down to 6 mm/day rather than 13 mm/day. This causes the background flow to reduce and beyond this convection appears to be modulated by a transient wave in a similar manner as in CW4A (discussed in the previous section).

(b) CWT3

This experiment was integrated forward for 60 days through July and August. Initially wave activity appears suppressed, the disturbance around day 15 being weaker in u than in CW4A but that in precipitation being similar (fig. 18). This spin-down of the westerly flow may be caused by switching on downdraught evaporation at the start of the integration, reducing convective heating by approximately 50% initially.

An increase in u_9 and convective rain occurs towards the end of July (around day 25 of the integration) linked to the passage of a second wave over the area. Moisture convergence moistens the atmosphere at this time (Fig. 19). During July the mean mixing ratio of the lowest model layer is 17.1 g/kg (c.f. 18.7g/kg in CW4A) while during August the mean value is 18.5g/kg. A moister lower atmosphere with a lower static stability than in CW4A (a potential temperature difference between layers 11 and 10 averaged over July and August of 0.5K compared to 1.3K for July of CW4A) allows sufficient convective heating to force the steady state circulation over the west Pacific. Study of $\underline{V}$, P_{MSL} and surface rainfall patterns for August of CWT3 indicates that the circulation is similar to that seen in the July of EVKS over the same area although the mean zonal wind at layer 9 over the area defined in section 6 is around 10 ms^{-1} compared to 15 ms^{-1} in EVKS.

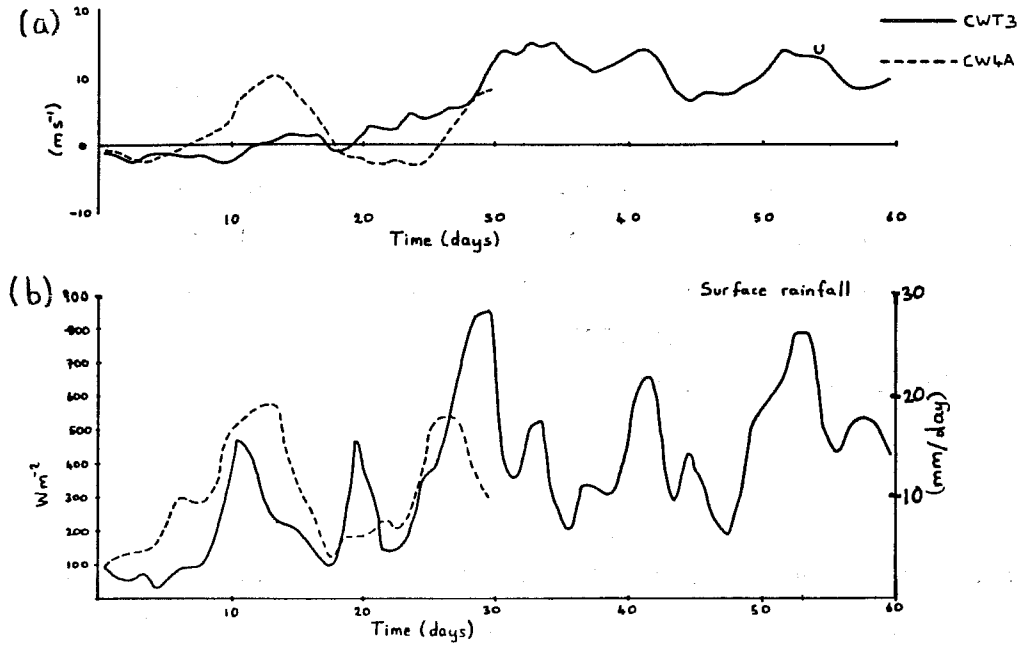

Fig. 18. Time series of (a) U at layer 9 and (b) convective precipitation for CWT3 and CW4A averaged over the West Pacific area for July and August.

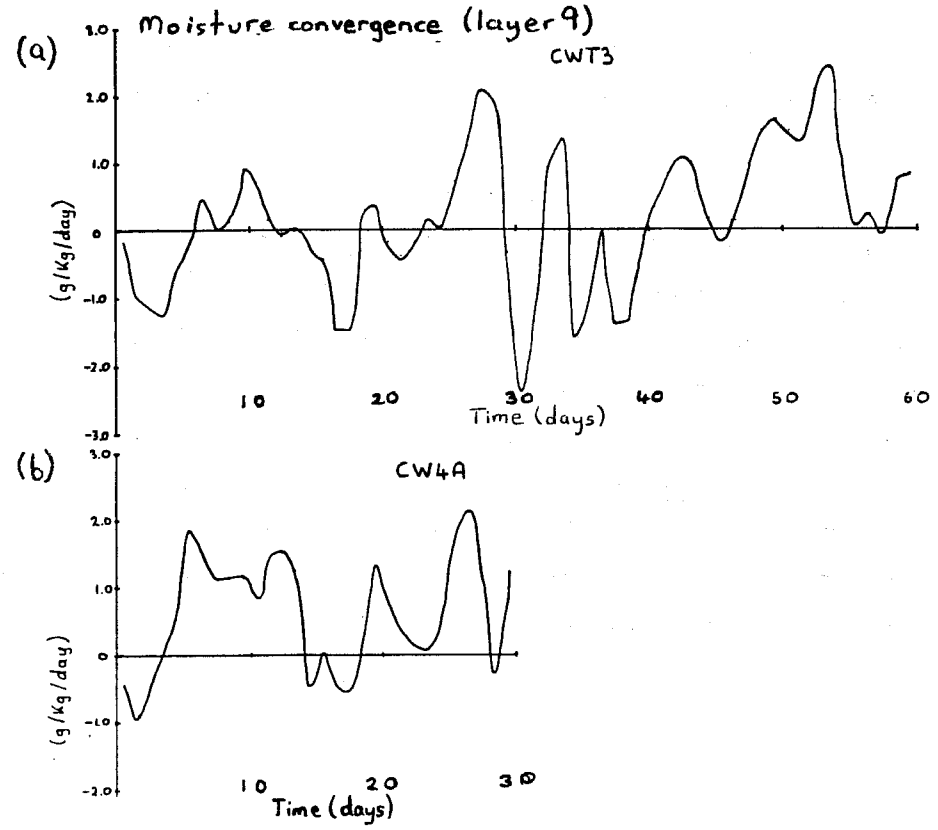

Fig. 19. Time series of dynamical moisture forcing at layer 9 for (a) CWT3 July, August and (b) CW4A July averaged over the West Pacific area.

Superimposed on the background flow are wave features. The precipitation time series has a similar profile as in EVKS with two peaks associated with the passage of each wave over the area. The period of the waves appear to be around 12 days, shorter than in previous integrations (around 18 days).

8. Further discussion and conclusions

It is clear from the integrations studied that a wave exists in the tropics of the 11-layer model with a period of around 18 days. Study of daily global fields suggest it is a transient form of the quasi-steady state circulation seen over the West Pacific in EVKS. Fig. 9 showed this to be similar to features seen in simple models of the tropical atmosphere in response to applied heating, which represent steady state Kelvin waves. Thus it seems reasonable to suggest that the transient waves are Kelvin waves.

Swinbank et al (1988) have used an aqua-planet version of the 11-layer model to study the 40 day wave observed in the tropical atmosphere. They found Kelvin waves propagating around the equator of the model, the structure of which resembled that of the 40 day wave although the modelled period was only 22 days. This is in agreement with other modelling studies of the 40 day wave which generally show the wave speed in AGCMs to be too great. Hayashi and Sumi (1986) using an aqua-planet model and Bruns et al, (1987) using a T21 version of the ECMWF model have found similar waves of a period between 20 and 30 days.

The wave period seen over the west Pacific is similar to that seen by Swinbank et al (1988). Initial study of time-longitude diagrams of 200 mb velocity potential (χ_{200}) averaged between the equator and 20°N for June, July and August of CW4A (not shown) suggest the west Pacific feature is a global phenomena. Minima in χ_{200} over the west Pacific (implying maximum divergence and convective activity) occur approximately at times when U_{850} peaks over the west Pacific (Fig. 11). Further minima over Central America and Africa are lagged behind those of the west Pacific by a period

corresponding to a wave travelling around the globe in an eastward direction approximately every 18 days. Although further research is needed to clarify the nature of the wave initial results suggest it is similar in nature to that seen by Swinbank et al (1988), being a Kelvin wave, and as such represents the model's attempt to simulate the 40 day wave.

The amplitude of the wave around 850 mb over the west Pacific is around 10 ms^{-1}, comparable with the 30 day mean wind speed over the area. Hence in order to simulate the climatology of the west Pacific well it would seem necessary to have a good representation of this transient feature.

The development of the stationary Kelvin wave over the west Pacific during July of EVKS is due to the interaction of the modified convection scheme and the 18 day wave. The modified convection scheme produces a more favourable environment for the growth and maintenance of convective heat release over this region, the model atmosphere having a lower static stability between layers 11 and 10 than with the fourth annual cycle scheme. Convection is initiated from layer 11 and so the buoyancy of a parcel lifted from this level to layer 10 will be greater with the modified scheme, leading to a larger initial convective mass flux (by eqn (1)) and so allowing the possibility of greater surface precipitation. The evaporation of falling precipitation within convective downdraughts also plays an important role in maintaining the steady convective heat release by offsetting drying due to dynamical forcing in some parts of the wave.

Whether the convection scheme employed in this study is too sensitive to the stability and moisture content of the lower layers of the model atmosphere is open to debate and it is planned to address this question further. Also transports of heat and moisture by downdraughts into the boundary layer are not represented in the convection scheme. These will cool and dry the boundary layer and so influence the static stability of the lower atmosphere.

The circulation seen during the July of EVKS over the west Pacific appears to be anomalous, not being found in any July between 1983 and 1986. However such features are seen over the West Pacific at other times of the year (e.g. Sept 1987). Thus it seems plausible that the interaction of the 40 day wave and a region favourable to convective growth (low static stability and a moist lower atmosphere) could force a stationary Kelvin wave over the west Pacific. Such a process may be important for the development of ENSO events. In a coupled atmosphere-ocean model an increase of westerly winds over the west Pacific would push the region of low winds usually associated with this region into the central Pacific (i.e. a reduction of easterly winds over the central Pacific). This would cause increased surface evaporation over the west Pacific, reducing sea surface temperatures while decreasing evaporation in the central Pacific hence increasing sea surface temperatures. Thus a region of warm water would appear to move from the west Pacific through to the central Pacific as seen in the ENSO cycle. Such a suggestion is very speculative but may be worth closer investigation.

The results presented indicate the importance of modelling transient planetary-scale features in the tropics of global models if they are to capture the observed flow well. The interaction of such features and diabatic forcing also appears of importance and is an area which deserves further investigation.

9. References

Bruns, T., Fischer-Bruns, I. and H. von Storch, 1987: The Structure and Propagation of Seasonal and Interseasonal Oscillations in the Tropical T21-Model Atmosphere., Large Scale Atmospheric Modelling, Report No. 1., Climate Simulations with the ECMWF T21-model in Hamburg., Ed. G. Fischer, Meteorologisches Institute der Universitat Hamburg., April 1987.

Carson, D.J., 1982a: Comments on the sensitivity of numerical simulations to different parameterizations of the boundary layer properties and processes., Met O 20 Technical Note II/186, Meteorological office, Bracknell.

Hartmann, D.L., Hendon, H.H. and Houze, R.A., Jr., 1984: Some Implications of Mesoscale Circulations in Tropical Cloud Clusters for Large Scale Dynamics and Climate., J. Atmos. Sci., 41, 113-121.

Hayashi, Y.-Y., and Sumi, A., 1986: The 30-40 day oscillation in an "aqua-planet" model. J. Met. Soc. Japan. II, 64, 451-467.

Kessler, E., 1969: On the distribution and continuity of water substance in Atmospheric circulation. Met. Monographs, 10, No. 32, A. Met. Soc., 84 pp.

Lin, Y.-L., Farley, R.D., and Orville, H.D., 1983: Bulk parameterizations of the snow field in a cloud model. J. Clim. and Appl. Meteor., 22, 1065-1092.

Palmer, T.N. and Mansfield, D.A., 1986: A study of wintertime circulation anomalies during past El Nino events, using a high resolution general circulation model II: Variability of seasonal mean response. Q. J. R. Met. Soc., 112, 639-660.

Phlips, P.J., and Gill, A.E., 1985: An analytic model of the heat-induced tropical circulation in the presence of a mean wind. Q. J. R. Met. Soc., 113, 213-236.

Reed, R.J. and Recker, E.E., 1971: Structure and properties of synoptic-scale wave disturbances in the equatorial West Pacific. J. Atmos. Sci., 28, 1117-1133.

Slingo, A. (Ed), 1985: Handbook of the Meteorological Office 11-layer atmospheric general circulation model. Volume 1: Model description. Description. Dynamical Climatology Technical Note 29, Meteorological Office, Bracknell.

Slingo, A. and Pearson, D.W., 1987: A comparison of the impact of an envelope orography and of a parameterization of orographic gravity-wave drag on model simulations., Q. J. R. Met. Soc., 113, 847-870.

Slingo, A. and Wilderspin, R.C., 1984: Development of a revised radiation scheme for an atmospheric general circulation model. Q. J. R. Met. Soc., 112, 371-386.

Smith, R.N.B., 1985: An integrated approach to the representation of cloud processes. ECMWF Workshop on Cloud Cover Parameterization in numerical models, 26-28 November, 1984.

Sommeria, G. and Deardorff, J.W., 1977: Sub grid-scale condensation in models of non precipitating clouds. J. Atmos. Sci., 34, 344-355.

Sundqvist, H., 1978: A parametrization scheme for non-convective condensation including prediction of cloud water content. Q. J. R. Met. Soc., 104, 677-690.

Swinbank, R., Palmer, T.N. and Davey, M.K., 1988: Numerical simulations of the Madden and Julian Oscillation. To be published in J. Atmos. Sci., January 1988.